Baku State University: Journal of Physics & Space Sciences, **2024**, v1 (3), p. 46-69

journal homepage: http://bsuj.bsu.edu.az/en

Ultrastructural characteristics of the accumulation of iron nanoparticles in intestine and liver of common carp (*Cyprinus Carpio* Linnaeus, 1758)

Chingiz A. Mammadov[*1], Aysel D. Hajiyeva[†2], Rovshan I. Khalilov[‡2]

[1]*Department of Zoology and Physiology, Faculty of Biology, Baku State University, Baku, Azerbaijan;*
[2]*Department of Biophysics and Biochemistry, Faculty of Biology, Baku State University, Baku, Azerbaijan.*

Received 17-Jul-2024; Accepted 05-Sep-2024
DOI: https://doi.org/10.30546/209501.2024.1.3.046

Abstract

Fe_3O_4 nanoparticles' accumulation in aquatic organisms, especially fish, and their induction of various pathological changes in the host organism have raised significant concerns. In our study on common carp, subjected to two different doses of Fe_3O_4 nanoparticles (10 and 100 mg per 10 g of food) for a 7-day period, notable alterations were observed in the intestine and liver. At a lower dose (10 mg), distinct changes like villi disintegration in the small intestine and cytoplasmic structure pathology in enterocytes were evident. Liver examination revealed alterations in erythrocytes, hepatocytes, canaliculi, and bile ducts. With a higher dose (100 mg), destructive changes occurred in all layers of the small intestine and the liver. Electron microscopy confirmed the sequential entry and bioaccumulation of Fe_3O_4 nanoparticles, starting from microvilli and traversing various cellular organelles. The observed nanoparticle size in fish intestine and liver structural elements was consistently up to 20 nm. These findings underscore the potential risks associated with Fe_3O_4 nanoparticles, emphasizing the need for further investigation into their environmental impact and implications for aquatic ecosystems.

Keywords: *Common carp, intestine, liver, nanoparticles, pathomorphological changes.*
PACS: 61.46.+w; UDK: 601.2

[*]e-mail: m_chingiz@yahoo.com; ORCID ID: 0000-0001-5785-2392.
[†]e-mail: ayselhaciyeva@bsu.edu.az; ORCID ID: 0009-0005-0705-046X.
[‡]e-mail: hrovshan@hotmail.com; ORCID ID: 0000-0002-8684-1390.

1. Introduction

In recent years, as a result of the large-scale increase in the production, use and application of nanomaterials, the risk of their waste spreading into the environment has increased. The spread of nanoparticles into water bodies – rivers and seas – causes a huge impact on ecosystems and their components [12] (p.20-22). Nanoparticles pose a threat to the environment and human health by spreading in the aquatic environment and accumulating in the body of living organisms in the ecosystem, including commercial fish [33] (p.723-727). Therefore, it is considered appropriate to select the above-mentioned particles as a biomodels of fish, which are used as human food. Common carp (*Cyprinus carpio* Linnaeus, 1758) is a fresh water fish, it is economically profitable due to its easy reproduction in commercial conditions and it is grown in many countries, including Azerbaijan. These fish are ideal models for studying animal ecology, developmental biology, and evolution [6] (p.353-358). There are more than 2,400 species in the *Cyprinidae* family [26] (p.). Despite this, it is common carp that has a share of 14% (3.4-4.0 million tons) among commercial fish (freshwater) grown in aquaculture worldwide [11] (p. 8542-8545). The sources of water used in fish farming farms are springs, rivers and other basins located in those areas. Those basins are polluted to a certain extent due to anthropogenic influences. Therefore, in recent years, the selection of fish as a biological, ecological, toxicological model has attracted the attention of many scientists [7] (p.1172-1179).

There are some studies testing various types of nanoparticles in free form or as metal oxides in model fish of carp [9, 12, 16, 24, 27, 37] (p. 207–210; p. 16-20; p. 100062; p. 863-869; p. 145-155; p. 209-212). The accumulation of various nanoparticles in different organs of the host (stomach, intestines, liver, blood-vascular system), their toxicity and some pathomorphological changes in carp fish under experimental conditions were studied in the sources mentioned above.

Nanoparticles of iron oxide have magnetic, catalytic properties. In addition, iron is one of the important components in the body of vertebrates and participates in carriage of breath, oxygen and electrons (transport), DNA synthesis and the formation of the immune system [1, p. 164–171). However, when its amount (concentration) in the body exceeds the norm, it can cause certain adverse effects (weakness of movement and vision, increase of haemoglobin, erythrocytes, haematocrit, decrease of leukocyte level, tissue damage) [1, 8, 30, 39] (p. 164–171; p. 3899-3905; p. 255-260; p. 1-6). Despite the above, there are few studies on the effects of metal nanoparticle oxides on fish [18] (p. 645-648).

Currently, large-scale scientific research is carried out by us in the territory of the country in the fields of study of the synthesis of free nanoparticles and with other compounds, their biological activity, practical application, bioaccumulation in various components of the ecosystem (soil, water, unicellular and multicellular organisms,

including various bacteria, molluscs, fish, etc.) and natural nanoparticles (ferritin) [2, 3, 13, 32, 35, 39] (p. 3258-3265; p. 41-45; p. 1711–1719; p. 101666; p. 114-120; p. 1-7).

Taking into account the above, the main objective of this research work is to determine the possible bioaccumulation of nanoparticles of iron oxide magnetite (Fe_3O_4) in various parts of the intestines of common carp (*Cyprinus carpio* Linnaeus, 1758), grown in aquaculture, and pathomorphological changes that occur in localization sites, with using light and electron microscopic methods.

2. Materials and methods

Selection of research objects and development of parameters

The primary stage of the research was conducted during June-July 2021 at the "Samukh-fish" farmer fishery in the Republic of Azerbaijan. The dimensions (L), weight (P), and fullness factor (F) of the experimental fingerlings were assessed using ichthyology-approved methods [26, 28] (p. 14-16; p. 33-36). In this study, 33 common carp (Cyprinus carpio Linnaeus, 1758) fingerlings (age 0+) served as biomodels to investigate the potential bioaccumulation of Fe_3O_4 nanoparticles in organs of organisms within the food chain, integral to the ecosystem. These carp fingerlings were nurtured in a fishery situated in the Neftchala district of Azerbaijan, and their diet consisted of artificial sturgeon feed in granule form.

Information about nanoparticles

Skyspring Nanomaterials in the course of experiments. Inc., USA, Houston TX. Fe_3O_4 (98+%, 10-30 nm, Product #: 3320DX) nanoparticles purchased from the company were applied.

Describing the experience

In September 2022, carp fingerlings transported to Baku were assessed for size and weight. They were segregated into three categories, each comprising 11 fingerlings, and allocated to three aquariums (1 control, 2 experimental) of equal volume (60 liters). The mean length (L) of the fingerlings placed in the tanks was 6.9 cm, with an average weight (P) of 4.9 g.

The experimental aquariums maintained consistent water volume (30 liters), hydrochemical parameters (t_0 – 22-24°C, O_2 – 8.2-8.6 mg/l, pH – 7.4-7.6), and daily feed ration (10 q). Group I (control) carp were exclusively fed artificial feed, while groups II and III (experimental) received daily feed with the addition of 10 mg and 100 mg of Fe_3O_4 nanoparticles, respectively. The experiments spanned 7 days, after which the small intestines of control (group I) and test (II and III) group fingerlings were dissected for examination.

Light and electron microscopic studies

The abdominal area of fingerling fish in both the control and experimental groups was incised using a scalpel. Subsequently, the small intestine from each fish was excised and fixed. The specimens were immersed in a solution comprising 2.5% glutaraldehyde, 2% paraformaldehyde, 4% surcosa, 0.1% picric acid, prepared in 0.1M phosphate buffer (pH=7.4). Following a one-day fixation period, the samples underwent postfixation in a 1% osmium tetraoxide solution in phosphate buffer (pH=7.4) for two hours. Araldite-Epon blocks were then fashioned from the material using standard electron microscopy techniques [21] (p. 799). Semi-thin sections (1-2 µm) obtained from these blocks with a Leica EM UC7 (Leica, USA) ultramicrotome were stained with methylene blue, azur II, and basic fuchsin or toluoid blue. These sections were observed under a Primo Star (Zeiss, Germany) microscope, and images of pertinent sections were captured using a digital camera EOS D650 (Canon, Japan) [9] (p. 207–210). Additionally, untreated sections from the same blocks, with a thickness of 50-70 nm, were scrutinized using a JEM-1400 (JEOL, Japan) transmission electron microscope at 80-120 kV, and electrograms were generated.

Determination of nanoparticles

During the examination of electrograms derived from ultrathin sections, prepared from unstained samples using the "Intensity profile" computer program, the horizontal line depicts structure length in nanometers, while the vertical axis represents gray values. It's essential to recognize that, similar to other monochrome images, electrogram intensity relies on varying shades of gray, with the lowest intensity fluctuating between black and the highest intensity. Our Veletta camera (Olympus, Germany) is equipped to process 14 bits of information per pixel, allowing it to distinguish 16384 different gray shades accurately. This capability ensures precise identification of nanoparticle locations within living organisms [35, 36] (p. 114-119; p. 243-251).

3. Results

Pathomorphological changes in the structure of the small intestine of common carp by exposure to iron nanoparticles

In order to study the bioaccumulation of nanoparticles in the body of carp, first of all, the ultrastructure of the small intestine and its layers in the norm was studied using light and electron microscopic methods, in order to compare the data obtained (Fig. 1). It should be noted that the small intestine is divided into 3 parts - front, middle and back, which differ in their morphological structure. Among the digestive organs, the middle part of the small intestine is longer than the others, where food digestion and absorption mainly take place. During our research, the

middle part of the intestine was studied. Figure 1A shows histological sections of the small intestine wall of common carp. As a result of research, it was found that the wall of the middle part of the small intestine of common carp consists of 4 layers: serosa (S), muscularis (ML), sub-mucosa (SM) and mucosa (MU) (Fig. 1A). Some of those layers, in turn, consist of several parts. In electrograms, serosa (S) consists

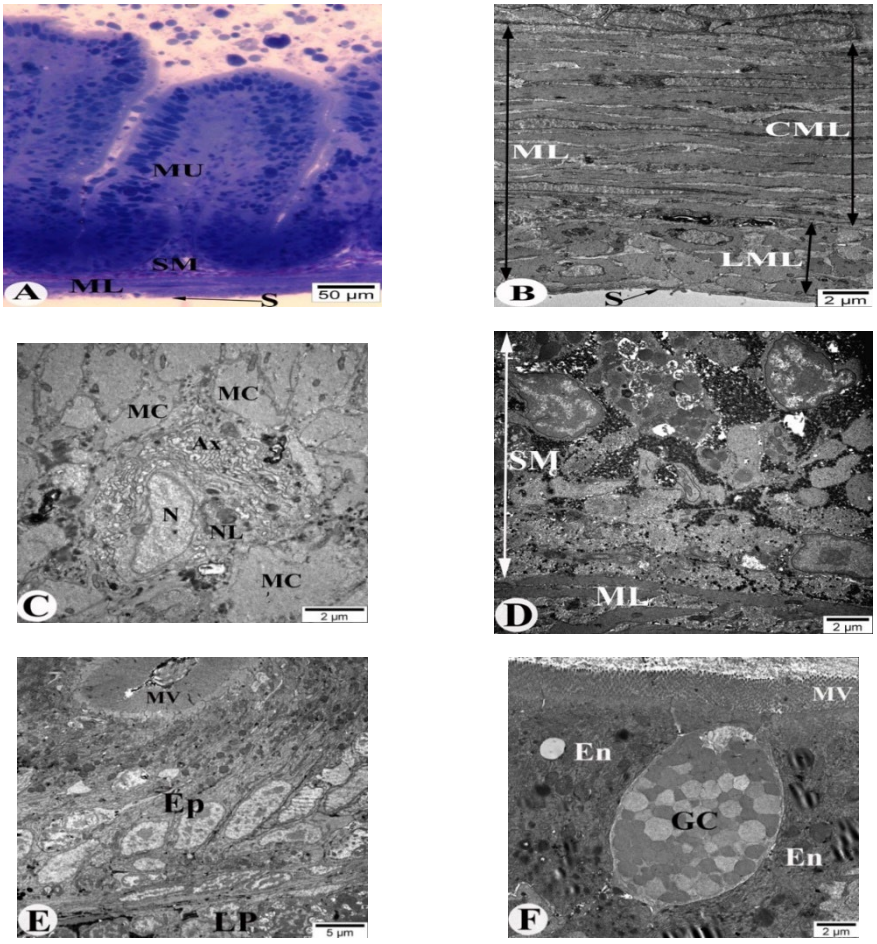

Fig. 1. Light and electron microscopic images of the small intestine of common carp in norm. A – General view of the intestinal wall. B – Serosa and muscularis layers (circular and longitudinal), C – Myenteric neural plexus, D – Structural elements of the sub-mucosa layer, E – Structural elements of the mucosa, F – Goblet cell in the epithelial layer. Designations: S – serosa, ML – muscularis, SM – sub-mucosa, MU – mucosa, N – nucleus, Ep – epithelium, LP – lamina propria, MV – microvilli, GC – goblet cell, En – enterocytes, CML – circular muscle layer, LML – longitudinal muscle layer, MC – muscle cell, NL - Schwann cell or neurolemmocyte, Ax – axon.

of single-layered mesothelial cells, with a large nucleus, mitochondria, endoplasmic reticulum, vesicles in their cytoplasm. Cells connected with each other with close junction (Fig. 1B). Moving towards to the lumen of the intestinal wall, there is a muscle layer after the serosa layer. It, in turn, is divided into longitudinal (LML) and circular (CML) muscle layers (Fig. 1B). Dense collagen fibers are observed between the muscle cells in both layers. In addition to the mentioned, the Myenteric neural plexus is observed between the muscle layers (Fig. 1C). In the center of the Schwann cell or neurolemmocyte, there is an oval-shaped nucleus composed of euchromatin and the nuclear envelope is clearly visible. In neurolemmocyte cytoplasm, Holci complex, lysosome, mitochondria, endoplasmic reticulum, etc. organelles are present. A large number of axons are located in pits around the plasmolemma of neurolymmocytes. They mainly contain neurofilaments and neurotubules, and sometimes sections of mitochondria and cisternae of the agranular endoplasmic reticulum (Fig. 1C). Beneath the muscle layer is the sub-mucosa (SM) layer (Fig. 1D). In this location, one can observe various connective tissue components, such as blood vessels, lymphocytes, macrophages, and other cell varieties, arranged in a structural manner. The last is the mucosa layer, which is divided into 3 structurally distinct parts: the epithelium (Ep), the lamina propria (LP) and the muscularis mucosa (Fig. 1E). The epithelial layer is composed of columnar cells, longitudinal enterocytes (En) and goblet cells (GC) (Fig. 1E and 1F). Enterocytes are terminated by microvilli at the lumen of the intestine (Fig. 1E and 1F). In the studied middle part of the small intestine, there are more goblet cells in the epithelial layer than in other parts, and the mucus they synthesize protects microvilli from damage by bacteria and toxic substances [14] (p. 115477).

After 7 days after iron nanoparticles were given in doses of 10 mg and 100 mg with food to common carps raised in aquaculture conditions, the small intestine was studied by light and electron microscopic methods and compared with the norm (Fig. 2). Initially, the impact of a 10 mg dosage of nanoparticles on distinct layers of the small intestine was investigated. Figures 2A and 2B present images of semi-thin (1 μm) sections of the intestinal mucosa, including the epithelium. In this context, pathomorphological alterations are noted in the apical regions of the epithelial cells oriented towards the intestinal lumen.

So, while the enterocyte microvilli (MV) were observed in the lateral parts of the intestinal folds, in those in the part facing the lumen, the completeness of the microvilli was disturbed, dispersed, and the structures in the cell cytoplasm, including fat droplets (FD) were scattered in the intestinal lumen (Fig. 2A and 2B). The mentioned processes are clearly observed in the electronograms obtained from the mentioned parts (Fig. 2C-2F). In the area indicated by the snowflakes in Figure 2C, the microvilli in the apical part of the enterocytes were completely destroyed. As a result of the pathomorphological changes that occur, it leads to a violation of the

intestinal absorption process in the mentioned areas. At high magnifications of the electron microscope, it is observed that the outer membranes of some organelles in the enterocyte cytoplasm, including mitochondria (Mt), are damaged, and inside the cristae are not clearly distinguished, and edema (marked with an asterisk) appears in the cytoplasm (Fig. 2D). In Figures 2E and 2F, it is observed that edema fluid (marked with an asterisk) is formed in the cytoplasm of enterocytes. In those pictures, it was also observed that the enterocytes that are close to the opening of the intestine are damaged, and the integrity of the wall of the epithelial cells that do not reach the opening is preserved (Fig. 2E and 2F). In the studies conducted by us, no serious pathomorphological changes were detected in other layers of the intestine after the application of 10 mg dose of nanoparticles.

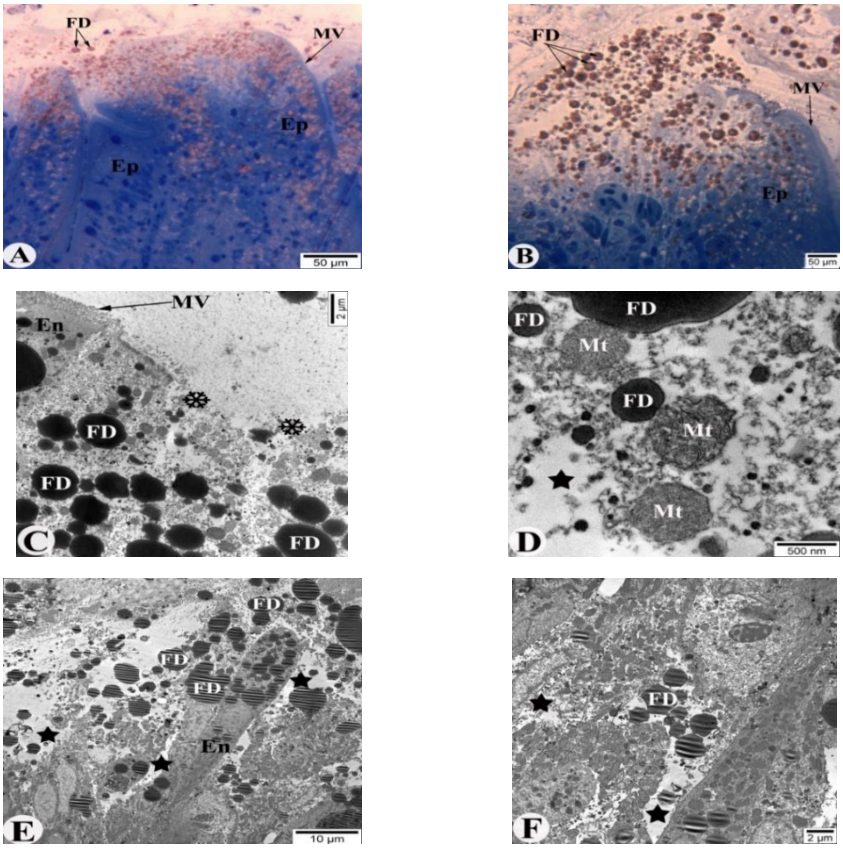

Fig. 2. Changes in the small intestine after exposure to Fe_3O_4 (10 mg) nanoparticles in common carp. A – B – Light microscope image of the mucosa layer of the small intestine, C – F – Electronograms of the epithelial cells and cytoplasmic organelles in the mucosa layer. *Designations*: Ep – epithelium, MV – microvilli, FD – fat droplets, En – enterocyte, Mt – mitochondrion, Star – edema.

Due to the effect of 100 mg dose of Fe_3O_4 nanoparticles, more serious changes occurred in the structure of the wall of the small intestine. Thus, pathology was observed in the serosa, muscularis and nerve elements, the sub-mucosa layer and the vessels located there (Fig. 3). In the electrogram presented in Figure 3A, it is clear that the serous layer is completely damaged and destroyed, and in the muscular layer, vacuolization and edema formation between the muscle cells are clearly visible. Mitochondria in the cytoplasm of muscle cells are swollen, structure of some of their cristas are broken. Due to the violation of the integrity of the membrane

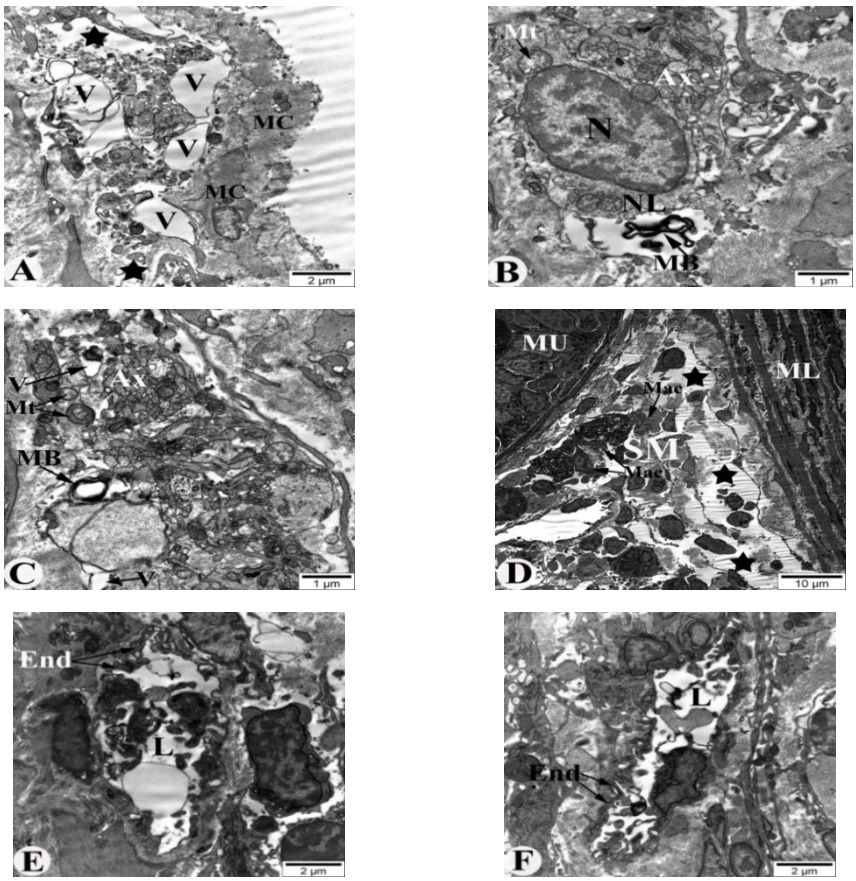

Fig. 3. Changes in the small intestine after exposure to Fe_3O_4 (100 mg) nanoparticles in common carp. A – Serosa and muscularis, B – C – Myenteric neural plexus, D – Sub-mucosa layer, E and F – Blood vessels in the sub-mucosa layer. *Designations*: V – vacuole, MC – muscle cell, NL - Schwann cell or neurolemmocyte, N – nucleus, Mt – mitochondrion, NL – Schwann cell or neurolemmocyte, Ax – axon, MB – myelin-like bodies, SM – sub-mucosa, ML – muscularis, MU – mucosa, Mac – macrophage, L – lumen of vessel, End – endothel of vessel, Star – edema.

structures in the cytoplasm of the neurolymmatocyte located between the muscle layers, myelin-like bodies of various shapes were detected, as well as vacuolization of the cytoplasm and swelling of the mitochondrial cristae, in addition, thickening of the nuclear membrane of the neurolymmatocyte was noted. The integrity of the basal membrane of unmyelinated nerve fibers is broken. In axons, there was an swelling of the granular endoplasmic reticulum (Fig. 3B and 3C). Edema fluid has formed between connective tissue elements in the sub-mucosa layer. In addition, a large number of macrophages are also observed (Fig. 3D). Changes in the ultrastructure of blood vessels were also found in the mentioned layer. It was observed that the endothelium covering the vessel wall from the lumen was deformed and the finger-like protrusions bulged towards the lumen (Fig. 3E and 3F). In the mucosa layer, as above, the integrity of the enterocytes was broken, the microvilli were fragmented and completely disintegrated in many places.

One of the tasks facing the research was to determine whether the used Fe_3O_4 nanoparticles of different doses enter the intestinal structural elements and bioaccumulate in them. Therefore, the enterocytes in the mucosa layer of the small intestine of common carp and the structural elements in the lamina propria, including the blood vessels, were studied separately under the 100,000-fold magnification of the electron microscope. As a result, it was found that Fe_3O_4 nanoparticles enter the microvilli located in the apical part of the enterocytes in the mucosa layer of the small intestine (Fig. 4A and 4B), from there to the cortical cytoskeleton part of the enterocyte (Fig. 4C and 4D), and then enter the cytoplasm of the epithelial (enterocyte) cell (Fig. 4E and 4F).

As a result of the study of the organelles in the cytoplasm of the enterocyte, it was determined that the used nanoparticles can also be collected in the cytoplasmic organelles. Thus, it was determined by us that the mentioned nanoparticles were also collected in the enterocyte nucleus, mitochondria, lysosomes and fat droplets [14] (p. 115477).

Nanoparticles were found during the examination of the lamina propria of the mucosa layer of the small intestine under the high magnification of the electron microscope, as well as in the cytoplasm of the endothelium, which forms the wall of the vessels in the lamina propria, and finally in the erythrocytes in the blood vessels.

It's important to highlight that the nanoparticles penetrating erythrocytes circulate within the body via the blood-vascular system. Furthermore, we provided visual representations for the accumulation of nanoparticles in the structural components of the small intestine along with corresponding diagrams for each depiction. Here, the degree of gray value varies between 5200-5400 with a slight difference regardless of the location of the nanoparticle. Thus, the introduction of Fe_3O_4 nanoparticles in the small intestine of the common çarp grown in aquaculture condi-

tions, starting from the microvilli located in the apical part of the enterocytes and directed towards the intestinal lumen, to the erythrocytes in the blood vessels which located in lamina propria, and their accumulation in various organelles in the cytoplasm of the cells was confirmed by electrograms and diagrams.

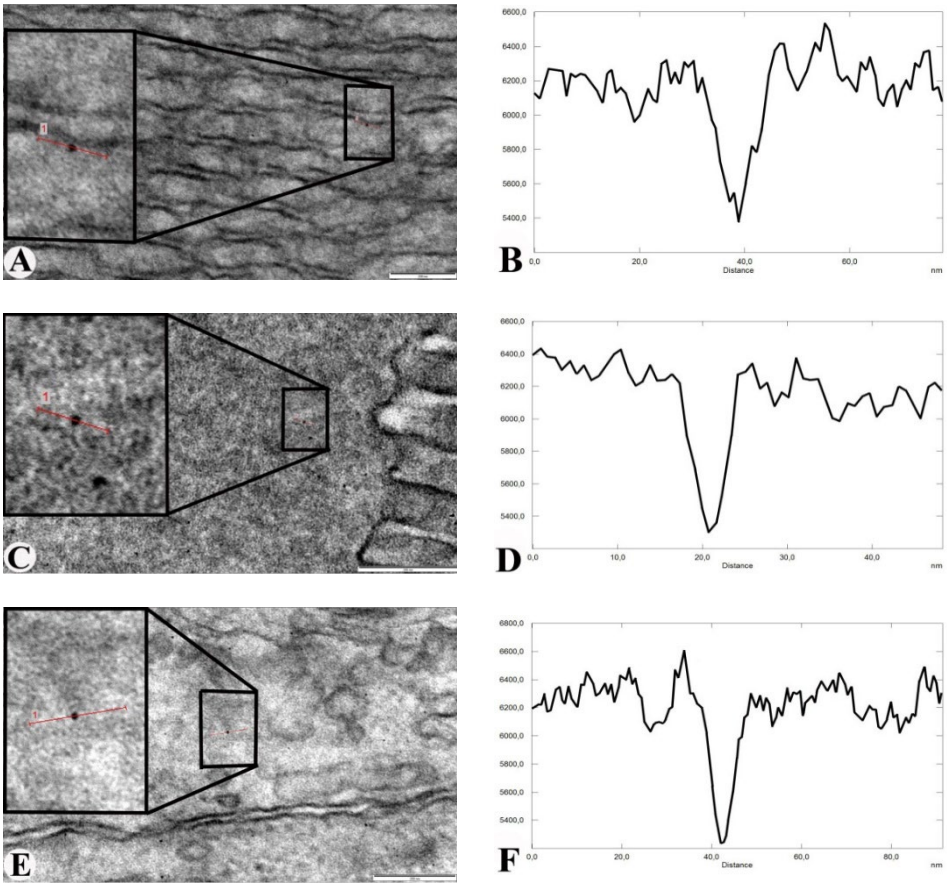

Fig. 4. Electron microscopic photos and corresponding diagrams of bioaccumulation of Fe_3O_4 nanoparticles in villi, cytoplasm and basal part of epithelial cells in the mucosa of the small intestine of common carp. A-B - In the intestinal villi, C-D – In the cortical cytoskeleton of the epithelium, E-F - In the cytoplasm of the epithelial cell.

Pathomorphological changes in the structure of the liver of common carp by exposure to iron nanoparticles

The ultrastructural examination of the common carp's liver was conducted using light and electron microscopic techniques under normal conditions and after ingestion of different doses (10 and 100 mg mixed with 10 g of feed) of Fe_3O_4 nanoparticles.

Initially, the study involved the control group of common carp. Figure 5A depicts the overall composition of a fish liver through a light microscope, showcasing clearly visible hepatocytes (H) and sinusoids (S) forming the liver parenchyma foundation.

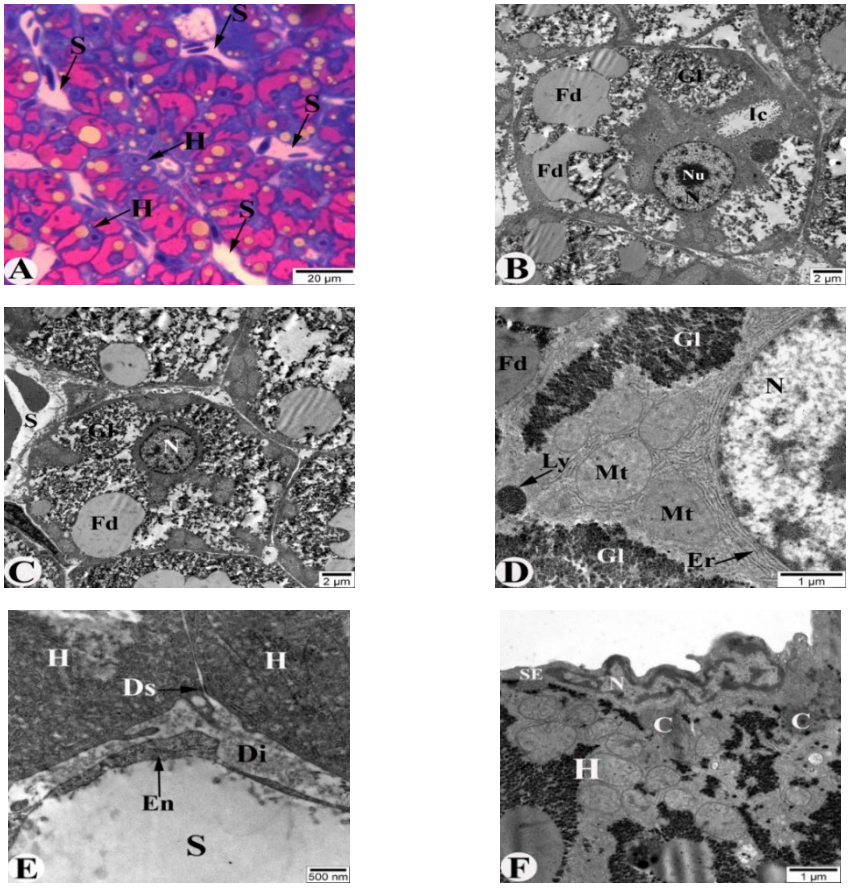

Fig. 5. Light and electron microscopic characteristics of the normal structure of the liver of common carp. A – a general view of the liver, B, C – an electron microscopic view of a hepatocyte, D – structural elements of the cytoplasm of a hepatocyte, E – desmosomes connecting hepatocytes with each other, F – simple squamous epithelium and connective tissue elements covering the liver from the outside. *Designations*: H – hepatocyte, S – sinusoid, Fd – fat droplets, Gl – glycogen, Ic – intracellular canaliculi, N – nucleus, Nu – nucleolus, Ly – lysosome, Mt – mitochondria, Er – endoplasmic reticulum, Ds – desmosome, Di – subendothelial space of Disse, En – endothelial cell, SE – simple squamous epithelium, C – callogen.

In 1 µm semi-thin sections of the common carp liver, irregular arrangements of vessels and hepatocytes were observed, lacking hepatic lobule division. The absence of portal triads was noted in the examined fish. Figures 5B and 5C present a

general perspective of a polygonal hepatocyte with a predominantly hexagonal shape in an electronogram. Both images reveal a centrally located hepatocyte with a large euchromatin-rich nucleus (N) and an electron-dense nucleolus (Nu).

The hepatocyte cytoplasm displays large fat droplets (Fd), glycogen (Gl), and intracellular canaliculi (Ic). At higher electron microscope magnifications (Fig. 5D), numerous organelles such as mitochondria (Mt), lysosomes (Ly), Golgi complex, phagolasosomes, granular endoplasmic reticulum (Er) around the nucleus, and a nuclear pore between the nucleus membranes become evident. Desmosomes (Ds) connect the membranes of hepatocytes (Fig. 5E). The fish parenchyma is externally covered by a simple squamous epithelium (SE) (Fig. 5F), featuring an elongated nucleus (N) and various cytoplasmic structures.

Connective tissue elements, represented by collagen bundles (C), are observed between the epithelial layer and hepatocytes, forming the composition of the liver capsule. Blood vessels, including sinusoids (S), are located between common carp liver hepatocytes, with the smallest vessels joining the central vein. Figures 6A and 6B specifically highlight the sinusoids, the blood vessels situated between hepatocytes.

Erythrocytes (E) and lymphocytes are situated within the sinusoidal lumen. The erythrocyte cytoplasm contains a large, round nucleus rich in euchromatin and heterochromatin. The sinusoid wall is comprised of a single layer of cells – the endothelium (En) (Fig. 5E and 6A). Endothelial cells, in turn, connect to each other through intercellular connections. A large nucleus (N) and cytoplasmic organelles - mitochondria, endoplasmic reticulum, ribosome, etc. are observed in the cytoplasm of the endothelium. The subendothelial space between the endothelium and hepatocytes is called the space of Disse (Di) (Fig. 5E and 6A). In addition to the above, hepatic stellate cells, also known as perisinusoidal cells or Ito cells (Hs), are also observed between sinusoids and hepatocytes (Fig. 6B). An irregularly shaped nucleus (N) and fat droplets (Fd) were found in the cytoplasm of those cells (Fig. 6B).

The liver, being the largest gland in the internal body of the carp fish, performs functions such as bile synthesis, glycogen storage, and lipid metabolism. Bile synthesis takes place in liver cells, that is, hepatocytes. In the cytoplasm of the hepatocyte, intracellular canaliculi (Ic) are present around the nucleus (Fig. 5B, 6C, 6D). They are formed as a result of intussusception of the hepatocyte membrane. There are numerous microvilli leading to the lumen of the intracellular canaliculi. Intracellular canaliculi membranes form tight connections with hepatocytes through desmosomes (Ds) (Fig. 6D). Intracellular canaliculi, in turn, open into biliary ductules between hepatocytes. The wall of these ductules consists of a single layer of biliary epithelial cells and has a large and elongated nucleus (N) (Fig. 6E). There is no basal lamina of the biliary ductules wall. They widen and open into the bile ducts (Fig. 6F). Bile ducts, unlike others, consist of several layers. Thus, in the obtained electrograms, it was observed that the wall of the duct is composed of peritubular cells

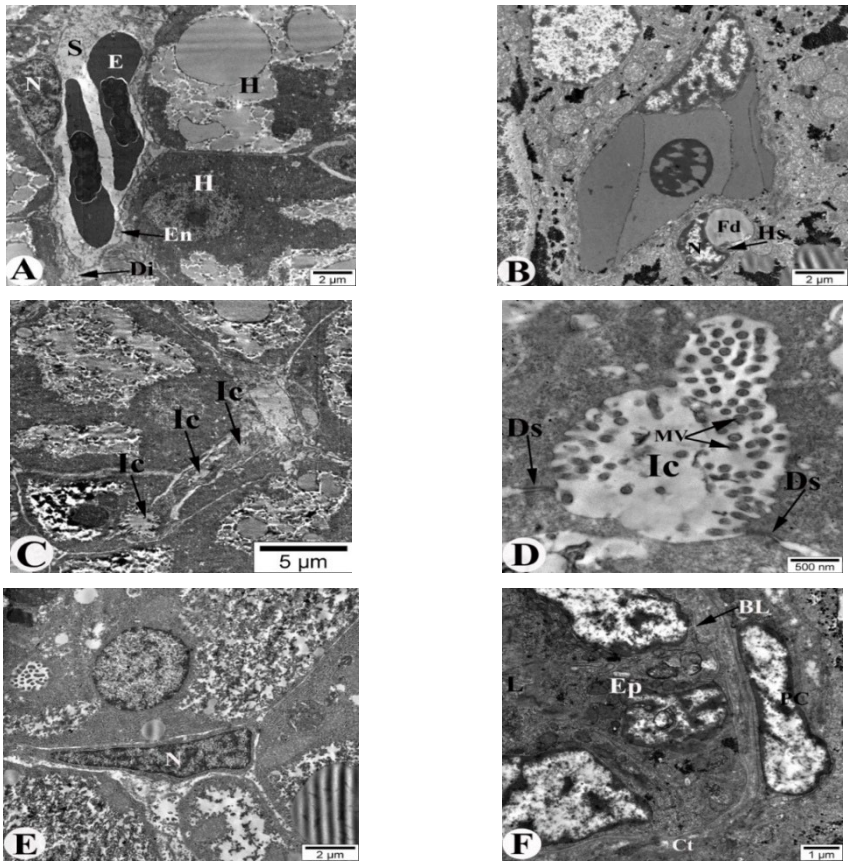

Fig. 6. Ultrastructural characteristics of the liver of common carp in norm. A – sinusoid structure, B – hepatic stellate cell, C – intracellular canaliculi in hepatocyte, D – intracellular canaliculi with desmosomes, E – nucleus of the epithelial cell of the biliary ductule wall, F – structure of the bile duct. Designations: H – hepatocyte, S – sinusoid, Fd – fat droplets, Ic – intracellular canaliculi, N – nucleus, L – lumen, Ds – desmosome, Di – subendothelial space of Disse, En – endothelial cell, Ep – epithelial cell, Ct – connective tissue, PC – peritubular cell, BL – basal lamina, MV – microvilla, Hs – hepatic stellate cell, E – erythrocyte.

(PC), connective tissue (Ct), basal lamina (BL), and epithelial layer (Ep) from the outside to the inside (Fig. 6F). The nucleus of epithelial cells is large, and the cytoplasm is rich in organelles. These cells are connected to each other through tight junctions. There are microvilli in the part of the epithelium that opens into the lumen (L).

After using different doses of Fe_3O_4 nanoparticles in the laboratory on common carp fish grown in aquaculture conditions, the fish's liver was studied by light and electron microscopic methods, initially using a dose of 10 mg. During the ultrastructural examination of the liver parenchyma, various degrees of pathomorphological

changes were observed in hepatocytes, including cytoplasmic organelles, blood vessels and erythrocytes, intracellular canaliculi, and bile ducts. Figure 7A shows a histological section of the liver. Here, hepatocytes and blood vessels are irregularly arranged, and the boundaries between cellular structures are not separated. Electronograms taken after exposure to 10 mg of Fe_3O_4 in the liver showed that cell membranes were not observed in many parts between hepatocytes, and intercellular borders were not detected in general (Fig. 7B). Changes in the cytoplasmic organelles of hepatocytes, including the nucleus (N), were observed at higher magnifications. Thus, the envelope of some nucleus is damaged, and in some parts it is broken (Fig. 7C).

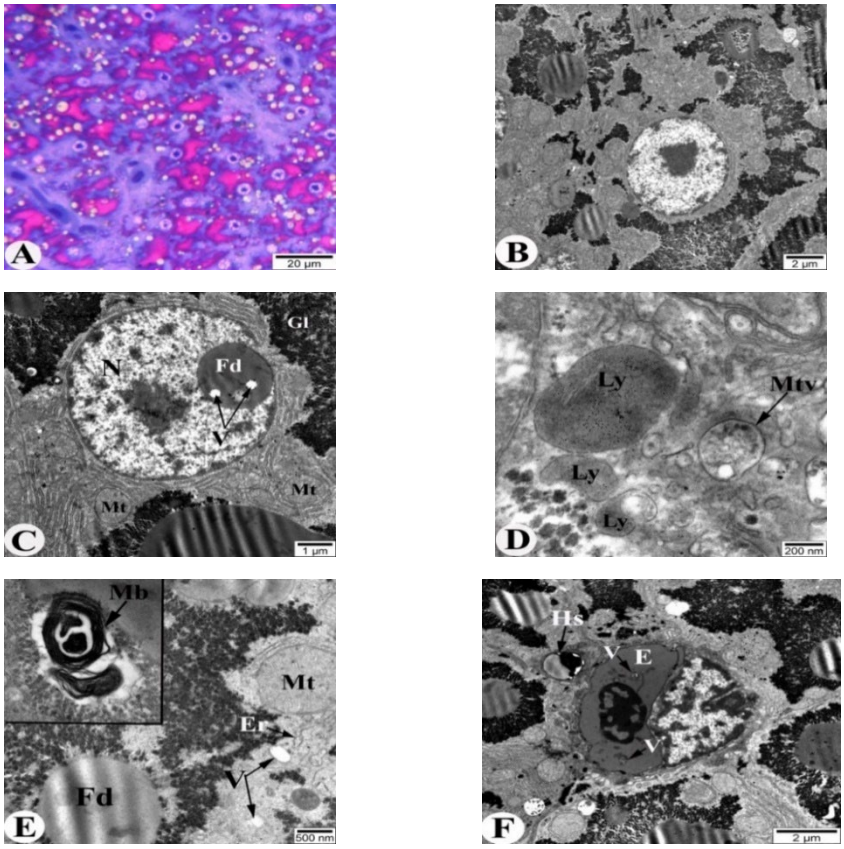

Fig. 7. Histological and ultrastructural characteristics of the changes occurring in liver hepatocytes and blood vessels after using a dose of 10 mg of Fe_3O_4 nanoparticles to common carp. A – histological view of liver parenchyma, B – general view of hepatocytes, C – changes in nucleus, D and E – changes in cytoplasmic organelles, F – changes in blood vessels and hepatic stellate cells. *Designations*: Fd – fat droplets, N – nucleus, Hs – hepatic stellate cell, E – erythrocyte, V – vacuole, Ly – lysosome, Mt – mitochondria, Er – endoplasmic reticulum, Gl – glycogen, Mb – myelin-like bodies, Mtv – multivesicular body.

As a result, some cytoplasmic structures - fat droplets (Fd) were able to enter the nucleus. The process of vacuolization (V) was also observed in the cytoplasm of fat droplets (Fig. 7C). An increase in the number of lysosomes (Ly) was also observed in the cytoplasm of hepatocytes. It is probably one of the defense mechanisms carried out by the cell due to the absorption and removal of nanoparticles inside the hepatocyte. In the electrogram obtained at 100,000 magnification of the electron microscope presented in Figure 7D, it is evident that a large amount of Fe_3O_4 nanoparticles is accumulated inside the lysosomes. In the cytoplasm, various cytoplasmic organelles are observed, including multivesicular bodies (Mtv), inside which vacuoles are also detected (Fig. 7D). In general, cytoplasmic structures with a membranous structure underwent changes and became myelin-like bodies (Mb) (Fig. 7E). In Figure 3E, the formation of vacuoles (V) was also observed in the cytoplasm of hepatocytes. The cisternae of the endoplasmic reticulum (Er) are swollen (Fig. 7E). Pathological processes were observed in the endothelium forming the wall of the sinusoids and in the cells around them due to the effect of the used nanoparticles.

Thus, the wall of the sinusoids is thinned and compressed. Vacuoles (V) were formed in the cytoplasm of erythrocytes (E) which located in the lumen of the vessel. The nucleus of hepatic stellate cells (Hs) located between hepatocytes and sinusoidal endothelium is degenerated (Fig 7F). Even at a small dose of nanoparticles used, it was observed that the membranes of the microvilli located at the lumen of the intracellular canaliculi (In), where the bile synthesized in the hepatocytes of the liver moves, undergo various changes and become osmiophilic structures (Os) (Fig. 8A). Bile ducts were also affected by pathological changes. Thus, the integrity of the nucleus of the cells in the epithelial layer was completely broken, the nuclear shell was destroyed and the remains of numerous membranes - myelin-like bodies (Mb) were observed. The chromatin in the nucleus is compressed or migrated to the cytoplasm. Mitochondria in the cytoplasm of epithelial cells are swollen, some of them are disintegrated, the crists of others are not clearly visible. In addition, myelin-like bodies (Mb) were formed due to changes in the membranous structures in the cytoplasm. Thus, myelin-like bodies (Mb) were found both in the cytoplasm of epithelial cells and in altered nuclei (Fig. 8B). Vacuolization was also observed in the cytoplasm of peritubular cells around the bile duct (Fig. 8B).

Hence, on the 7^{th} day following the administration of 10 mg of Fe_3O_4 nanoparticles, detrimental alterations were noted in hepatocytes and their cytoplasmic organelles, microvilli, various layers of bile ducts, erythrocytes within blood vessel lumens, hepatic stellate cells located between hepatocytes and endothelium, and intracellular canaliculi formed by invagination of hepatocyte membranes.

The impact of a 100 mg dose of (Fe_3O_4) on common carp's liver was also investigated using both light and electron microscopic methods, as illustrated in Figure 9. Figure 9A provides an overview of the liver and blood vessels from semi-thin sections (1 μm).

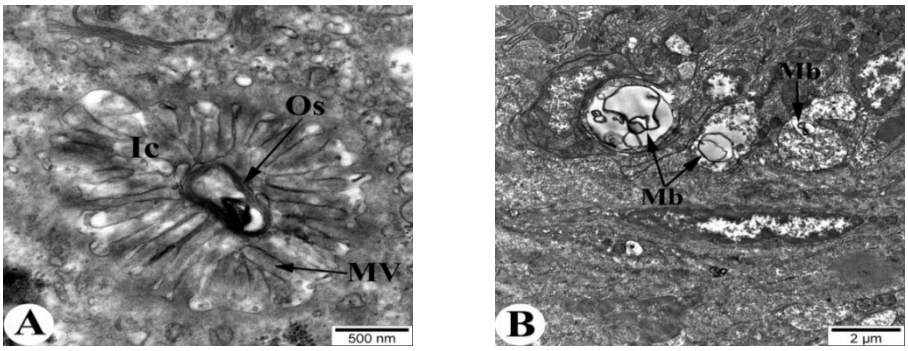

Fig. 8. Ultrastructural characteristics of the changes in the intracellular canaliculi and bile ducts of the liver due to the use of a dose of 10 mg of Fe_3O_4 nanoparticles to common carp. A – changes in the bile capillary, B – changes in the bile duct. *Designations*: Os – osmiophil structures, Ic – intracellular canaliculi, MV – microvilla, Mb – myelin-like bodies**.**

In this context, the hepatocytes exhibit irregular arrangement, and their cytoplasm appears transparent with abundant vacuoles. The electrogram in Figure 5B illustrates the thickening of the flat single-layer epithelium surrounding the liver, accompanied by the presence of edema fluid. In some areas, the epithelium is completely destroyed, leading to the dispersion of cytoplasmic organelles due to cell integrity disruption (Fig. 9B). Another electrogram (Fig. 5C) reveals pathological processes within hepatocytes, showcasing damaged membranes and disintegration, causing a mix of cytoplasmic organelles between hepatocytes. Electron microscopic examination exposes damaged, compressed, and degenerated nuclei (Fig. 9D). The endothelial wall is thinned and damaged, and the space of Disse is scarcely observed. Erythrocytes in sinusoids show perinuclear expansion, thickened nuclear envelopes, and concentrated heterochromatin at the nucleus edges (Fig. 9E). Pathological changes in biliary ductules include undefined connections between epithelial cells, damaged cytoplasmic organelle membranes, and the presence of small vacuoles. Microvilli membranes opening into the lumen part of the ductules are damaged, forming myelin-like bodies (Fig. 9F). Consequently, the administration of 100 mg of Fe_3O_4 nanoparticles for seven days induces severe pathological changes in the fish liver, encompassing capsule damage, hepatocyte and organelle disintegration, blood vessel wall damage, edema formation, and disruptions in biliary ductule structures.

The research aimed to investigate the bioaccumulation and incorporation of Fe_3O_4 nanoparticles into the liver's structural components in common carp fries. The examination, conducted at a 100,000 magnification with an electron microscope, focused on distinct elements such as blood vessel walls, erythrocytes, hepatocyte cytoplasm, organelles, intracellular canaliculi, and liver ducts. Following

fish consumption, nanoparticles, ingested with varying doses of food, entered through small intestine microvilli, traversing vessels in the mucous layer's lamina propria. Subsequently, they circulated through various organs, including the liver. Electron microscopy of the liver revealed nanoparticle presence in erythrocyte cytoplasm within sinusoid lumens (Fig. 10A and 10B), endothelial cells forming sinusoid walls (Fig. 10C and 10D), and hepatocyte cytoplasm (Fig. 10E and 10F).

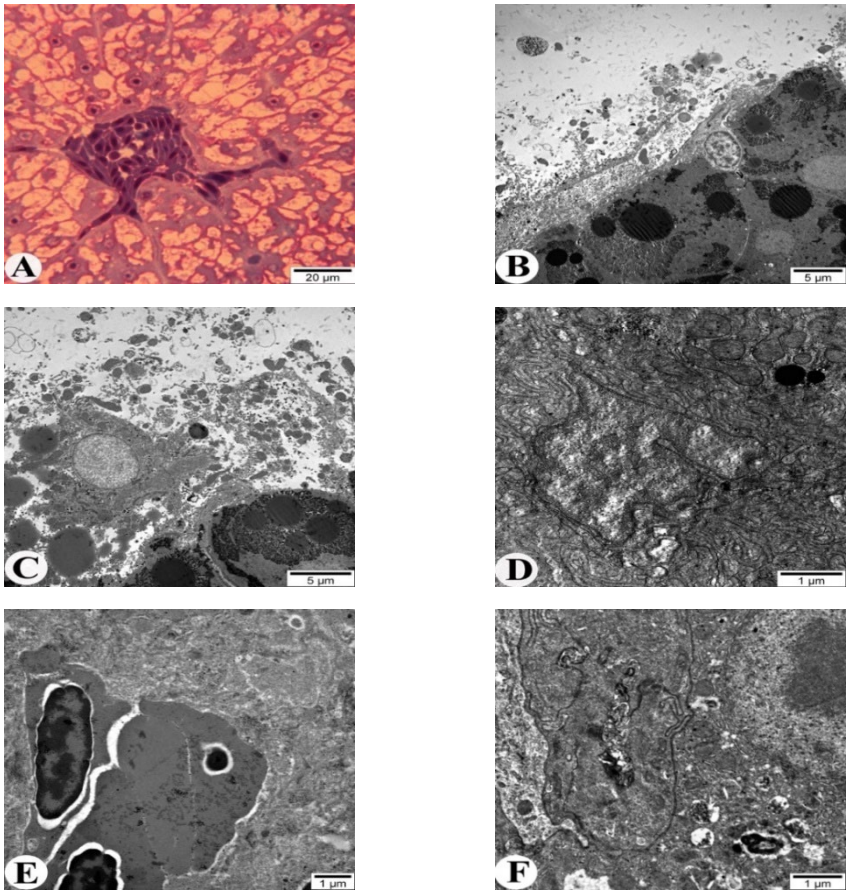

Fig. 9. Histological and ultrastructural characteristics of the degenerative changes in the liver due to the use of a dose of 100 mg of Fe_3O_4 nanoparticles to common carp. A – histological view of parenchyma, B – changes in the capsule of the liver, C and D – changes in hepatocyte and cytoplasmic organelles, including the nucleus, E – changes in erythrocytes, F – changes in the bile duct.

In addition to freely dispersing within hepatocyte cytoplasm, the utilized nanoparticles were observed to penetrate cytoplasmic organelles. Consequently, bioaccumulation was identified in the central nucleus of hepatocytes, lysosomes, mito-

chondria, and glycogen. Beyond these findings, Fe_3O_4 nanoparticles were also detected in the microvilli directed towards the lumen of intracellular canaliculi within

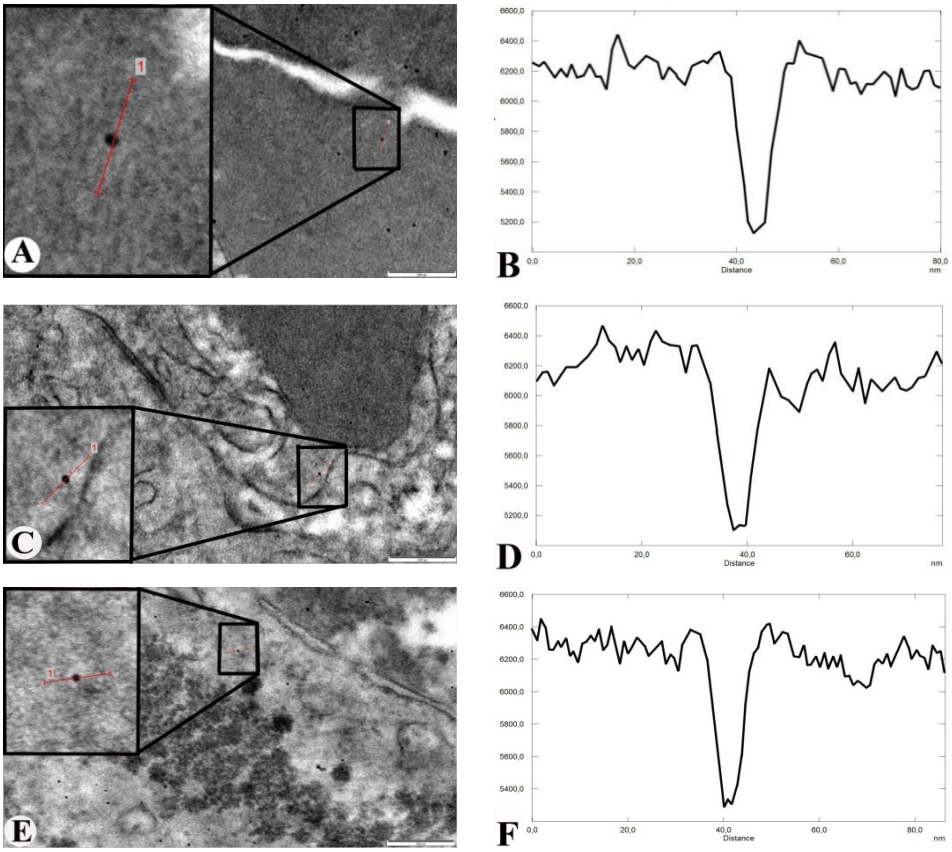

Fig. 10. Electron microscopic images and corresponding diagrams of the bioaccumulation of Fe_3O_4 nanoparticles in the cytoplasm of the erythrocytes, endothelium, and hepatocytes in the sinusoid wall of the liver of the common carp. A-B - in the erythrocyte in the sinusoid lumen of the liver; C-D - in the endothelium forming the wall of the sinusoid of the liver; E-F - In the cytoplasm of the hepatocyte of the liver.

liver hepatocytes and within the structural components of bile ducts. Specifically, nanoparticles were present in the basal layer of bile ducts, in the cytoplasm of cells in the epithelial layer, and within the bile duct lumen. It's noteworthy that, along with the provided electronograms detailing the bioaccumulating aspects of nanoparticles, histograms displaying grey value and structure length (in nm) have been included. These histograms consistently reveal minimal grey value fluctuations (5100-5300), implying the same particle - the Fe_3O_4 nanoparticle. Notably, the size of these nanoparticles ranges between 10-20 nm. This confirms that Fe_3O_4 nano-

particles, endowed with magnetic properties, traverse the common carp's liver, entering from erythrocytes in blood vessels and progressing through the vessel endothelium, hepatocytes (including cytoplasmic organelles), intracellular canaliculi, and bile ducts, all validated through electron microscopic analysis.

4. Discussion and conclusion

The investigation into the normative structure of digestive organs, particularly the small intestine in common carp, involved histological and electron microscopic methods [33] (p. 721–730). Summarizing the findings, it's noteworthy that the small intestine wall comprises four layers: serosa, muscularis, sub-mucosa, and mucosa. In examining the small intestine's structure, all mentioned layers were identified through various methods (Fig. 1). These layers, as established, further subdivide into distinct components. For instance, the mucosa layer delineates into epithelial (enterocyte and goblet cells), lamina propria, and muscularis mucosa segments (Fig. 1). Similar observations were made in the mucosa layers of the small intestine in other bony fishes studied, such as Catla catla, Anguilla anguilla, Clarius batrachus, Salmo salar, Oncorhynchus mykiss, Serrasalmus nattereri [2, 10, 24, 30, 37] (p. 3258-3264; p. 477-484; p. 859-872; p. 255-260; p. 209-212). The small intestine's muscular layer is characterized by two muscle types (circular and longitudinal muscle layers) (Fig. 1B), with the Myenteric neural plexus, a component of the enteric nervous system, present between them. Our findings also revealed neurolymocytes or Schwann cells and unmyelinated nerve fibers (Fig. 1C), aligning closely with the research of other scientists on nerve elements between the muscular layers of the common carp's small intestine [15, 19] (p. 147-158; p. 27-39).

Additionally, beyond functioning as a detoxifying organ in fish, the intestines serve as a pivotal indicator of the host's health status and the pathways through which nanoparticles infiltrate organisms [23] (p. 10). This perspective positions it as a model for assessing the toxic characteristics of diverse nanoparticles in commercial fish and investigating resultant pathomorphological alterations in the body. Literature analysis reveals that the introduction of certain nanoparticles (such as CuO, Fe_2O_3, Fe_3O_4, ZnO, multi-walled carbon nanotubes (MWCNTs), etc.) to common carp elicits histological and ultrastructural changes primarily in the intestine, liver, spleen, kidney, skin, muscle, and blood vessels [4, 12, 20, 22, 24, 28, 38] (p. 85-94; p. 15-20; p. 109005; p. 9–15; p. 859-870; p. 33-38; p. 108832). Notably, the application of copper (CuO) nanoparticles induces oxidative stress in common carp, manifesting destructive modifications in the liver and kidney [12] (p. 15-20). Similarly, the impact of other metal oxide (ZnO) nanoparticles is observed in the nuclei of liver hepatocytes, glomeruli, and kidney channels in common carp [22] (p. 109005). Our use of iron oxide nanoparticles in common carp has been documented in the literature, detailing alterations in various organs (stomach, liver,

muscle, skin, scales), including the intestines [4, 20, 25, 28] (p. p. 85-94; p. 109005; p. 41-50; p. 33-38). Some studies indicate that iron nanoparticles may induce immunotoxicity by accumulating in the small intestine and liver of fish [20] (p. 109005). Depending on dosage and duration, pathological changes are evident in the small intestine of common carp, with observations of degeneration of intestinal villi, structural integrity breaches, reduced villus count, intestinal wall thinning, epithelial cell swelling, and disrupted intercellular junctions. Despite sustained high-dose administration, there's a marked reduction in nanoparticle levels in the common carp body after the 21st day.

The authors highlighted that disruptions in the mechanism of nanoparticle entry into enterocytes, involving endocytosis and subsequent passage through intestinal layers via exocytosis into the blood-vascular system, result from the listed pathomorphological changes [28] (p. 33-38). In contrast to previous studies, our use of iron nanoparticles at relatively high doses (10 mg and 100 mg per 10 g of food) led to early pathomorphological changes, evident in enterocytes within the mucosa layer of the small intestine on the 7th day, as observed through light and electron microscopic methods at a 10 mg dose (Fig. 2). Microvilli integrity in enterocytes facing the lumen was disrupted, and structural elements, including fat droplets, scattered into the intestinal lumen (Fig. 2A and 2B). These changes were corroborated by electrograms (Fig. 2C-2F). Additionally, damage to the outer membranes of mitochondria, unclear cristae, and cytoplasmic edema in enterocytes were noted (Fig. 2D). At the 100 mg dose, pathological changes extended to all layers of the intestine after 7 days, encompassing serosa, muscularis, nerve elements, sub-mucosa layer, and vessels. Complete serosa layer damage, muscular layer vacuolization, edema between muscle cells, nerve element integrity loss, sub-mucosa layer edema, endothelium deformation, and enterocyte damage and destruction were identified (Fig. 3). Our analysis, considering literature data and our research results, indicates that nanoparticle dose and duration of exposure dictate the intensity of pathomorphological changes in the host's body. Notably, our study on common carp revealed varied changes in erythrocyte nuclei in vessels based on the dose of Fe_3O_4 nanoparticles. Following our use of Fe_3O_4 nanoparticles, the lamina propria of the intestinal wall and vessel lumens in the sub-mucosa layer exhibited disrupted coating of erythrocyte nuclei, cytoplasmic vacuolation, and deformation of some erythrocytes.

Metal nanoparticles exhibit distinct patterns of accumulation in the body, determined by their size. Notably, 4 nm nanoparticles predominantly accumulate in the kidneys, while those within the range of 10-28 nm bioaccumulate in the stomach and small intestine walls. Larger nanoparticles are entrapped by the mucus produced by goblet cells in the epithelial layer of the digestive system, often remaining in the mucous layer without penetrating deeper layers. Transmission Electron Mic-roscope (TEM) studies reveal that nanoparticles sized 10-30 nm can traverse the lamina propria, reaching connective tissues, endothelium, and even erythrocytes in vessels, subsequently dispersing to various organs. Despite using 10-30 nm Fe_3O_4 nanoparticles, TEM images indicate observation of only 10-20 nm nanoparticles in intestinal villi, enterocyte cytoplasm, organelles, endothelial cells, and erythrocytes. This aligns with findings in other research on iron nanoparticles in the small intestine of rainbow trout. The crucial role of nanoparticle size in cellular and tissue entry is emphasized by both literature and our research. Our study on common carp raised in aquaculture con-

ditions investigates the ultrastructural aspects of iron oxide nanoparticle entry and bioaccumulation in the small intestine and liver. Exposure to different nanoparticle doses (10 and 100 mg) results in dose-dependent damage, ranging from destruction of enterocytes at a low dose to comprehensive pathomorphological changes in all layers of the intestinal wall at a high dose. Nanoparticles, particularly those up to 20 nm, traverse microvilli, enter enterocyte cytoplasm, and subsequently navigate through the mucosa layer, lamina propria, endothelium, and erythrocytes, ultimately spreading to other organs.

Acknowledgments: *We appreciate Professor E.K. Gasimov and Associate Professor F.H. Rzayev of Azerbaijan Medical University for their contributions to the conducted study and valuable recommendations.*

References

[1] Abbaspour, N.; Hurrell, R.; Kelishadi, R. Review on iron and its importance for human health. Journal of Research in Medicine Sciences, 2014, Volume 19 (2), pp. 164–174.

[2] Agayeva N.J.; Rzayev F.H.; Gasimov E.K.; Mamedov Ch.A.; Ahmadov İ.S.; Sadigova N.A.; Khusro A.; Al-Dhabi N.A.; Arasu M.V. Exposure of rainbow trout (*Oncorhynchus mykiss*) to magnetite (Fe_3O_4) nanoparticles in simplified food chain: Study on ultra-structural characterization // Saudi Journal of Biological Sciences, 2020, Volume 27 (12), pp. 3258-3266. https://doi.org/10.1016/j.sjbs.2020.09.032

[3] Ahmadov I.S.; Qasimov E.K.; Sadiqova N.A.; Agayeva N.J.; Rzayev F.H.; Manafov A.A. Transfer of nanoparticles in a simplified aquatic food chain: from water plant Elodea canadensis to molluscs Lymnaea auricularia // Journal of Low Dimensional Systems, 2018, v. 2 (2), pp. 41-45.

[4] Alijantabar, M.; Omidzahir, Sh.; Kardel, F. Study of iron bioaccumulation and histopathology of muscle, skin and scale of common carp (Cyprinus carpio) following exposed to iron oxide nanoparticles. Journal of Agriculture Development, 2022, V. 6 (1), pp. 85-98, https://doi.org/10.52547/aqudev.16.1.85

[5] Bergin, I.L.; Witzmann, F.A; Nanoparticle toxicity by the gastrointestinal route: evidence and knowledge gaps. Int J Biomed Nanosci Nanotechnol., 2013, V. 3(1-2), doi:10.1504/IJBNN.2013.054515

[6] Bongers, A.B.; Sukkel, M.; Gort, G.; Komen, J.; Richter, C.J. Development and use of genetically uniform strains of common carp in experimental animal research. Laboratory Animals, 1998, V. 32, pp. 349-363. https://doi.org/10.1258/002367798780599749

[7] Burgos-Aceves, M.A.; Lionetti, L.; Faggio, C. Multidisciplinary haematology as prognostic device in environmental and xenobiotic stress-induced response in fish. Sci. Total Environ. 2019, V.670, p.1170-1183. https://doi.org/10.1016/j.scitotenv.2019.03.275.

[8] Chen PJ; Wu WL; Wu KCW. The zerovalent iron nanoparticle causes higher developmental toxicity than its oxidation products in early life stages of medaka fish. Water Res. 2013; V.47(12), p. 3899-3909. https://doi.org/10.1016/j.watres.2012.12.043

[9] D'Amico F. A polychromatic staining method for epoxy embedded tissue: a new combination of methylene blue and basic fuchsine for light microscopy. Biotech Histochem

2005; V.80(5–6) pp. 207–210. doi: 10.1080/10520290600560897

[10] Domeneghini, C.; Arrighi, S.; Radaelli, G.; Bosi, G. and Veggetti, A. Histochemical analysis of glycoconjugate secretion in the alimentary canal of Anguilla anguilla L. Acta Histochemica. 2005, V.106 (6), pp. 477-487. doi: 10.1016/j.acthis.2004.07.007

[11] Fiorino, E.; Sehonova, P.; Plhalova, L.; Blahova, J.; Svobodova, Z.; Faggio, C.;. Effects of glyphosate on early life stages: comparison between Cyprinus carpio and Danio rerio. Environ. Sci. Pollut. Res. 2018, p.8542-8549.

https://doi.org/10.1007/s11356-017-1141-5.

[12] Gupta, Y.R.; Sellegounder, D.; Kannan, M.; Deepa, S.; Senthilkumaran, B.; Basavaraju, Y. Effect of copper nanoparticles exposure in the physiology of the common carp (Cyprinus carpio): Biochemical, histological and proteomic approaches. Aquaculture and Fisheries, 2016, V. 1(1), pp. 15-23.

http://dx.doi.org/10.1016/j.aaf.2016.09.003

[13] Hajiyeva S.; Hasanova U.; Gakhramanova Z.; Israyilova A.; Ganbarov Kh.; Gasimov E.; Rzayev F.; Eyvazova G.; Huseynzada A.; Aliyeva G.; Hasanova I.; Maharramov A. The role of diazacrown ether in the enhancement of the biological activity of silver nanoparticles. Turkish Journal of Chemistry, 2019, V.43: pp. 1711–1721. TÜBİTAK

doi:10.3906/kim-1907-10

[14] Hajiyeva, A.; Mamedov, Ch.; Gasimov, E.; Rzayev, F.; Khalilov, R.; Ahmadian, E.; Eftehari, A.; William C. Ultrastructural characteristics of the accumulation of iron nanoparticles in the intestine of Cyprinus carpio (Linnaeus, 1758) under aquaculture. Ecotoxicology and Environmental Safety, 2023, V. 264, p. 115477.

https://doi.org/10.1016/j.ecoenv.2023.115477

[15] Halasy K.; Benedeczky I.; Fekete E.; Toth L.; Gabiel R. Enteric neuromuscular junctions: comparison of ultrastructural features in different phylogenetic groups. Neuroscience. 1988, V.25(1), pp.147-62.

doi: 10.1016/0306-4522(88)90014-0

[16] Jha N.; Annamalai A.; Essakiraj P.; Balamurugan R.; Lakra A.K.; Tilwani Y.M.; Arul V. Effects of polysaccharide-based silver and selenium nanoparticles on growth perfor-mance, biochemical parameters, and immune response of Cyprinus carpio. Fish and Shellfish Immunology Reports 3, 2022, pp. 100062.

https://doi.org/10.1016/j.fsirep.2022.100062

[17] Kadhim, Kh. H.; Karim, A. J.; Kadhim, Kh. K. Histological and histochemical study of the liver and gall bladder of adult male common carp Cyprinus carpio. Plant Archives. 2020, V.20 (1), pp.438-442.

[18] Karthikeyeni S.; Siva Vijayakumar T.; Vasanth S.; Ganesh A.; Manimegalai M.; Subramanian P. Biosynthesis of iron oxide nanoparticles and it haematological effects on fresh water fish Oreochromis mossambicus. J Acad Indus Res. 2013, V.1(10), pp. 645-649.

[19] Katalin H.; István B. Electron microscopic study on the innervation of the gut-musculature in the carp (*Cyprinus carpio*). Acta biologica, 1985, V.(31) 1-4. pp. 27-42.

[20] Khoei, A.J.; Evaluation of potential immunotoxic effects of iron oxide nanoparticles (IONPs) on antioxidant capacity, immune responses and tissue bioaccumulation in common carp (*Cyprinus carpio*). Comparative Biochemistry and Physiology, Part C, 2021, V. 244, pp. 109005.

https://doi.org/10.1016/j.cbpc.2021.109005

[21] Kuo, J.; Electron microscopy: methods and protocols. Totowa: Humana Press, 2014, pp.799. DOI 10.1007/978-1-62703-776-1

[22] Lee J.; Kim J.; Shin Y.; Ryu J.; Eom İ.; Lee J.S.; Kim Y.; Kim P.; Choi K.; Lee B. Serum and ultrastructure responses of common carp (Cyprinus carpio L.) during long-term exposure to zinc oxide nanoparticles. Ecotoxicology and Environmental Safety, 2014, V.104, pp. 9–17 http://dx.doi.org/10.1016/j.ecoenv.2014.01.040

[23] Lee J.W.; Choi Y.Ch.; Kim R.; Lee S.K. Multiwall Carbon Nanotube-Induced Apoptosis and Antioxidant Gene Expression in the Gills, Liver, and Intestine of Oryzias latipes. BioMed Research International, 2015, Article ID 485343, 10 p.

http://dx.doi.org/10.1155/2015/485343

[24] Lokka. G.; Austbo, L.; Falk, K.; Bjerkas, I. and Koppang, E.O. Intestinal morphology of the wild Atlantic salmon (Salmo salar). J Morphol. 2013, V.274, pp.859-876.

doi: 10.1002/jmor.20142

[25] Movahed M.M., Babakhani A., Sattari M., Ghafouri H., Johari S.A. Effects of iron oxide nanoparticles (Fe2O3) on the antioxidant defense system and lipid peroxidation in the gill of juvenile common carp (Cyprinus carpio). Aquatic Physiology and Biotechnology, 2019, 7(1),

[26] Najafov, S.A.; Mammadov, Ch. A.; Hajiyev, R.V. Fishing, fish feeding and ichthyopathology. Baku, Muallim, 2019, 304 p. (In Azerbaijanian)

[27] Nelson, J.S.; Fishes of the World. 4th ed. Hoboken, NY, USA: John Wiley and Sons, Inc. 2006, pp: 135-165.

[28] Omidzahir S.; Alijantabar Bayi M.; Kardel F.; Mazandarani M. Effects of iron oxide nano-particles on the intestinal tissue of Common carp, Cyprinus carpio. Iran J Toxicol. 2019; V.13 (3), pp. 33-38.

[29] Pravdin I.F. Guide to the study of fish. Moscow, Food Industry, 1966, pp. 375 (In Russian)

[30] Raji, A.R. and Norouzi, E. Histological and histochemical study on the alimentary canal in walking catfish (Claris batrachus) and piranha (Serrasalmus nattereri). Iranian. J. Vet. Res., 2010,V.3: pp. 255-261. Doi:10.22099/IJVR.2010.130

[31] Remya, A.S.; Ramesh, M.; Saravanan, M.; Poopal, R.K.; Bharathi, S.; Nataraj, D. Iron oxide nanoparticles to an Indian major carp, Labeo rohita: impacts on hematology, iono regulation and gill Na + /K + ATPase activity. J King Saud Univ Sci. 2015, V. 27(2), pp. 151-60. https://doi.org/10.1016/j.jksus.2014.11.002

[32] Rzayev F.H.; Gasimov E.K.; Agayeva N.J.; Manafov A.A.; Mamedov C.A.; Ahmadov I.S.; Khusro A.; Valan Arasu M.; Sahibzada M.U.K.; Al-Dhabi N.A.; Choi K.C.. Microscopic characterization of bioaccumulated aluminium nanoparticles in simplified food chain of aquatic ecosystem. Journal of King Saud University - Science, 2022, doi: https://doi.org/10.1016/j.jksus.2021.101666

[33] Sabeeh H.T.; Alshami I.J.J.; Al-Tameemi R.A. Histochemical study of the intestine in the common carp Cyprinus carpio fingerlings to detect the impact of replacement of dietary fish and soybean meals with shrimp wastes. Egyptian Journal of Aquatic Biology & Fisheries. 2021, Vol. 25(2), pp.721 – 734. DOI: 10.21608/ejabf.2021.169190

[34] Saravanan M.; Suganya R.; Ramesh M.; Poooal R.K.; Gopalan N.; Ponpandian N. Iron oxide nanoparticles induced alterations in haematological, biochemical and ionoregulatory responses of an Indian major carp Labeo rohita. J Nanopart Res. 2015, V.17(6), pp. 274. Doi: 10.1007/s11051-015-3082-6

[35] Shadlinskaya R.V.; Gasimov E.K.; Rzayev F.H; Some results of light-optical and electron-microscopic study of the elements of the lamina propria of the mucous membrane of the free part of

the gums in patients with β-thalassemia major. Azerbaijan Medical Journal, special issue, 2020, 114-121.

[36] Smith S.W. The Scientist & Engineer's Guide to Digital Signal Processing.1st Edition. USA: California Technical Publishing, 1997, 640p.

[37] Suresh, N. and Ranganathan, S. Studies on the histoarchitecture of the gastrointestinal tract of Catla catla (Hamilton). Aquaculture. 2003, V.4(2), pp. 209-213.

[38] Tavabe K.R.; Yavar M.; Kabir S.; Akbary P.; Aminikhoei Z. Toxicity effects of multi-walled carbon nanotubes (MWCNTs) nanomaterial on the common carp (Cyprinus carpio L. 1758) in laboratory conditions. Comparative Biochemistry and Physiology, Part C 237 (2020), p. 108832. https://doi.org/10.1016/j.cbpc.2020.108832

[39] Valiyeva G.G.; Palma L. Di.; Hajiyeva S.R.; Ramazanov M.A.; Hajiyeva F.V.; Gasimov E.K.; Rzayev F.H. Reuse of bimetallic nanoparticles for nitrate reduction. IEEE Transactions on Nanotechnology, 2022, pp. 1-8. DOI: 10.1109/TNANO.2022.3230284

[40] Van der Oost R.; Beyer J.; Vermeulen N.P. Fish bioaccumulation and biomarkers in environmental risk assessment: A review. Environ Toxicol Pharm. 2003, V. 13(2), pp.57-149. doi: 10.1016/s1382-6689(02)00126-6.